

# **Sub-Nanosecond Electrical Pulse Switching of an Easy Plane Antiferromagnetic Insulator**

Justin J. Michel, Jose Flores, and Fengyuan Yang

Department of Physics, The Ohio State University, Columbus, OH 43210, USA

## **Abstract**

Electrical switching of antiferromagnets (AFM) is critical for AFM spintronics. However, there is an active debate about the mechanisms of observed AFM switching on whether the switching is due to spin-orbit torques or the much slower thermally-induced magnetoelastic effect. We report reliable current-induced AFM switching in Pt/ $\alpha$ -Fe<sub>2</sub>O<sub>3</sub> bilayers using electrical pulses with various durations down to 0.3 ns. The dependence of switching threshold current density on the pulse width indicates that spin-orbit torques are the dominant mechanism responsible for electrical switching of AFMs in the ns regime, reaffirming AFM spintronics as a promising field for ultrafast and ultrahigh-frequency applications.

In recent years, research in spintronics has focused increasingly on AFM insulators due to their potential advantages, such as lack of stray magnetic fields, low damping, ultrafast dynamics, and electrical switching driven by spin-orbit torques (SOT).<sup>1-10</sup> However, despite experimental demonstrations of electrical switching of the Néel vector in heavy-metal (HM)/AFM-insulator bilayers, the mechanisms of AFM switching remain elusive.<sup>11-17</sup> There is an ongoing debate on whether the observed electrical switching of AFM insulators is primarily driven by the thermally-induced magnetoelastic effect (ME), which requires a slow process of heating, or by SOT, which is expected to occur at picosecond (ps) to nanosecond (ns) timescales.<sup>13, 14, 18, 19</sup> This is further complicated by the presence of nonmagnetic switching-like signals due to resistance change of the HM layer.<sup>20-22</sup> In this sense, the future of antiferromagnetic spintronics is largely dependent on whether SOTs alone can result in AFM switching. One of the most direct ways to decouple the two aforementioned mechanisms is to achieve electrical switching of AFM insulators using ultrashort (e.g., sub-ns) electrical pulses, for which the thermal effects become negligible.

AFM insulator  $\alpha$ -Fe<sub>2</sub>O<sub>3</sub> has generated much interest in this field due to its low anisotropy, high Néel temperature, and a low spin-flop transition magnetic field (<1 T) which allows control of its AFM spins by a magnetic field, in addition to electrical pulses. This ability is essential for sub-ns electrical switching due to the required impedance matching (50  $\Omega$ ) for delivery of such ultrashort pulses. In this letter, we report reliable electrical switching of Néel order in Pt/ $\alpha$ -Fe<sub>2</sub>O<sub>3</sub> bilayers using electrical pulses with various durations down to 0.3 ns, which is our instrument limit. The ultrafast electrical switching and the threshold current densities for switching at various pulse widths demonstrate that in this sub-ns regime, the dominant mechanism for electrical switching of AFM insulators is SOT rather than thermally-driven magnetoelastic effect.

We grow  $\alpha$ -Fe<sub>2</sub>O<sub>3</sub>(15 nm) epitaxial films on Al<sub>2</sub>O<sub>3</sub> (0001) substrates using off-axis

sputtering as described previously.<sup>15, 23</sup> Then, a 4-nm Pt layer is deposited on  $\alpha$ -Fe<sub>2</sub>O<sub>3</sub> at room temperature using off-axis sputtering. For ultrashort pulse measurements, we fabricate a Hall cross structure by patterning the Pt layer into an electrical switching channel (1.5  $\mu$ m wide) aligned along Al<sub>2</sub>O<sub>3</sub>[1 $\bar{1}$ 00] with 0.5  $\mu$ m wide Hall electrodes using electron-beam lithography and reactive-ion etching. Next, we pattern and deposit two 100-nm thick silver contacts onto the two ends of the current channel with a 1.5  $\mu$ m gap, which reduces the channel resistance to 56  $\Omega$ . A scanning electron microscopy image and a schematic of the Hall cross are shown in Fig. 1(a).

To deliver sub-ns electrical pulses to our device with minimal loss, we use the circuit shown in Fig. 1(a). A fast rise-time (70 ps) voltage pulse generator with a minimum pulse width ( $\Delta t$ ) of 300 ps sends an ultrashort pulse current ( $I_P$ ) for switching. A DC current source sends a sensing current ( $I_S$ ) for Hall measurement detected by a nanovoltmeter. Both the pulse generator and DC sourcemeter are connected to an RF switch box, which can selectively connect either one to a coplanar waveguide (CPW) with a 50  $\Omega$  impedance wire-bonded to our device.

We first check the circuit's pulse performance by measuring voltage pulses with an output voltage of 1 V and varying widths delivered through our CPW and measured by a 6 GHz oscilloscope as shown in Fig. 1(b), which exhibits no significant attenuation for pulses down to 0.3 ns (the small attenuation is attributed primarily to imperfect impedance matching). Since the Hall leads have significantly higher resistance ( $\sim 2$  k $\Omega$ ), the pulse current spreading into these leads is negligible. Thus, in this work, the pulse current is calculated from  $V/R$ , where  $V$  is the output pulse voltage from the pulse generator and  $R = 56 \Omega$ .

To demonstrate magnetic field control of the AFM states in our device, we measure the in-plane angular dependence ( $\alpha$ ) of transverse spin magnetoresistance (TSMR),  $R_{xy}$  (also referred to as Hall resistance), at room temperature. Figure 1(c) shows the  $\sin 2\alpha$  angular dependence of  $R_{xy}$

at  $\mu_0 H \geq 0.3$  T, indicating that at a moderate magnetic field, the AFM spins in the  $\alpha$ -Fe<sub>2</sub>O<sub>3</sub> film are almost fully aligned perpendicular to the magnetic field in the (0001) plane via the spin-flop transition. Thus, our pulse measurements described below utilize a 0.5 T magnetic field to initialize the alignment of AFM spins.

Typical AFM switching experiments rely on multiple current channels for electrical alignment of the Néel vector along different directions.<sup>11, 14, 15, 24</sup> However, such multi-channel structures with a thin Pt layer exhibit resistances much larger than 50  $\Omega$  as required for delivery of ns pulses. Here, by taking advantage of field control of AFM spins in  $\alpha$ -Fe<sub>2</sub>O<sub>3</sub> films, we fabricate a Pt/ $\alpha$ -Fe<sub>2</sub>O<sub>3</sub> device with  $\sim 50$   $\Omega$  impedance, where the Néel vector can be aligned by a 0.5 T field to a desired orientation before electrical switching with ns pulses. In addition, the current density in our current channel is more uniform than those with multiple current channels.<sup>11, 13-15</sup>

Electrical pulse measurements are performed on our Pt/ $\alpha$ -Fe<sub>2</sub>O<sub>3</sub> device at room temperature with the following steps. First, we apply an in-plane magnetic field of 0.5 T at  $\alpha = 30^\circ$  to align the AFM spins in the perpendicular direction as shown in Fig. 2(a), and then ramp the field down to zero. As described in our previous work,<sup>15</sup> this leaves the  $\alpha$ -Fe<sub>2</sub>O<sub>3</sub> film in a multidomain remnant state with a preferred orientation of Néel vector along  $\alpha = 120^\circ$ . Subsequently, we measure  $R_{xy}$  5 times using a sensing current  $I_s = 100$   $\mu$ A along  $x$ -axis with a 3 s wait in between, which gives a stable  $R_{xy} \approx 4$  m $\Omega$  as shown in Fig. 2(b) (blue points). Next, we send an electrical pulse through the current channel, wait 10 s, and measure  $R_{xy}$  again (red points). Such pulse-measure sequence is performed 5 times with a 3 s wait between sequencies. Finally, a 0.5 T in-plane field is applied again at  $\alpha = 30^\circ$  to realign the AFM spins along  $\alpha = 120^\circ$  and then ramped back down to zero before the next set of measurements (blue points). This procedure is repeated multiple times for each pulse width, resulting in a clear step-like switching signal over a

wide range of pulse widths of  $\Delta t = 0.3, 1, 5,$  and  $50$  ns with current densities ( $J_p$ ) of  $1.1 \times 10^{13}, 8.3 \times 10^{12}, 5.7 \times 10^{12},$  and  $3.5 \times 10^{12}$  A/m<sup>2</sup>, respectively, as shown in Figs. 2(b)-(e).

If the observed AFM switching is caused by the damping-like SOT, the electrical pulse tends to rotate the Néel vector towards  $x$ -axis (parallel to the pulse current), which is expected to result in a negative  $R_{xy}$  change from the field-aligned state (blue points) to the pulse-switched state (red points). This pulse switching corresponds to the field-controlled AFM spin rotation in Fig. 1(c) from  $\alpha = 30^\circ$  to  $90^\circ$  ( $\alpha = 90^\circ$  results in AFM spins aligned along  $x$ -axis), which exhibits a saturated  $\Delta R_{xy} = -16$  m $\Omega$ . We note that the remnant AFM state is multiple domains with a preferred spin orientation either after the field is ramped back to zero or after the electrical pulse is applied. Therefore, the measured remnant-state  $R_{xy} = -4$  m $\Omega$  is a fraction of the saturated value of  $-16$  m $\Omega$ .

The AFM switching results in step-like signals in the measured  $R_{xy}$  as can be seen in Figs. 2(b)-(d) for  $\Delta t = 0.3$  to  $50$  ns. In addition, nonmagnetic effects have been shown to appear in the switching measurements by multiple investigations.<sup>21, 22</sup> This typically exhibits sawtooth-like switching signals, where successive electrical pulses continuously change  $R_{xy}$ , likely due to electromigration of grain boundaries in the thin Pt layer.

To further confirm the magnetic origin of the AFM switching driven by ultrashort electrical pulses, we reduce the alignment magnetic field from  $0.5$  to  $0.1$  T and perform the pulse switching measurement with  $\Delta t = 0.3$  ns, as shown in Fig. 2(f). This small field of  $0.1$  T is well below the in-plane spin-flop transition field of our  $\alpha$ -Fe<sub>2</sub>O<sub>3</sub> films, which is not strong enough to align the AFM spins. As a result, we observe essentially no change in the measured Hall resistance, confirming the magnetic origin of the electrical switching.

Several mechanisms have been proposed to explain the current-induced magnetic switching in AFMs, while the primary debate is on whether it is driven by SOT or thermally-

induced magnetoelastic coupling. In order to decouple the heating-related effects from SOT, we conduct a systematic investigation of the dependence of switching on pulse width and amplitude. For each measurement sequence with a certain pulse width, we initialize the alignment of AFM spins by an in-plane field of 0.5 T. After the field is ramped back to zero, we send pulses of the same  $\Delta t$  with increasing current density and measure  $R_{xy}$  after each pulse. Figure 3(a) shows four such sequences with  $\Delta t = 0.3, 1, 5,$  and  $50$  ns. For each  $\Delta t$  sequence, there is a threshold pulse current density ( $J_{th}$ ), below which  $R_{xy}$  remains at a high value of  $\sim 4$  m $\Omega$ , indicating no AFM switching. Above the  $J_{th}$ ,  $R_{xy}$  abruptly decreases to a  $\sim 0$  m $\Omega$ , indicating AFM switching. This demonstrates the existence of a specific threshold current density for each pulse width.  $J_{th}$  has a clear dependence on  $\Delta t$ , as larger current densities are needed to switch the AFM for shorter  $\Delta t$ .

To investigate the dependence of  $J_{th}$  on  $\Delta t$ , we repeat the measurements for a wide range of  $\Delta t$  up to 200 ns. Figure 3(b) shows the obtained  $J_{th}$  as a function of  $\Delta t$  from 0.3 to 200 ns, where each data point is the average of 5 measurements. For  $\Delta t < 2$  ns,  $J_{th}$  follows a  $1/\Delta t$  dependence, as shown in the  $1/\Delta t$  vs.  $J_{th}$  plot in Fig. 3(c), which is the same trend seen in ferromagnetic systems resulting from an intrinsic switching mechanism related to the conservation of angular momentum.<sup>25-28</sup> Using the angular momentum transfer model for SOT switching in ferromagnets, we fit Fig. 3(c) by  $J_{th} = J_{th0} + Q/\Delta t$ , from which we extract  $J_{th0} = 6.4 \times 10^{12}$  A/m<sup>2</sup> and  $Q = 1.1 \times 10^3$  C/m<sup>2</sup>. Here,  $Q$  is the effective charge parameter that describes the efficiency of charge to angular momentum transfer.  $J_{th0}$  represents the minimum pulse current density needed to overcome the anisotropy barrier and damping. For  $\Delta t > 2$  ns,  $J_{th}$  is lower than what is expected from the  $1/\Delta t$  behavior. This effect has also been observed in ferromagnetic SOT switching, and can be explained by thermally-assisted switching, where the pulse current generates sufficient heat in the device to help overcome the anisotropy energy barrier.

To evaluate the contribution of thermal effects on the electrical pulse switching of our  $\alpha$ -Fe<sub>2</sub>O<sub>3</sub> films, we simulate the temperature ( $T$ ) rise in our devices using COMSOL (see Supplementary Information for details) for several threshold pulse current densities based on the measured pulse profiles in Fig. 1(b). Between  $\Delta t = 0.3$  and 200 ns, we obtain a maximum temperature rise of 0.17 to 3.6 K from our simulations, as shown in Fig. 3(d). At  $\Delta t \leq 1$  ns, the temperature rise is well below 1 K. In addition, the active heating area in our device is a  $1.5 \times 1.5$   $\mu\text{m}^2$  square as shown in Fig. 1(a), which is not expected to result in an anisotropic strain. Thus, we conclude that spin-orbit torque is the primary mechanism for electrical switching of the Néel vector in our  $\alpha$ -Fe<sub>2</sub>O<sub>3</sub> films in the sub-ns regime.

In summary, we achieve sub-ns electrical pulse switching of AFM spins in Pt/ $\alpha$ -Fe<sub>2</sub>O<sub>3</sub> bilayers. The threshold current density varies from  $3.0 \times 10^{12}$  A/m<sup>2</sup> for 200 ns pulses to  $9.9 \times 10^{12}$  A/m<sup>2</sup> for 0.3 ns pulses. Our COMSOL simulations indicate that the temperature rise is negligible for the sub-ns regime, excluding the thermally-driven magnetoelastic effects as the mechanism for the observed electrical switching of AFM spins. The confirmation of spin-orbit torques as the primary mechanism for electrical control of AFMs in the sub-ns timescales is a critical step toward realizing the promises of AFM-based spintronic technologies.

This work was supported by the Department of Energy (DOE), Office of Science, Basic Energy Sciences, under Grant No. DE-SC0001304.

## Figure Captions:

**Figure 1.** (a) Schematic of the switching circuit and device of a Pt(4 nm)/Fe<sub>2</sub>O<sub>3</sub>(15 nm) bilayer with a  $1.5 \times 1.5 \mu\text{m}^2$  cross area and 0.5  $\mu\text{m}$  wide Hall leads (inset: SEM image). The Pt layer is etched into a Hall cross and 100-nm thick silver is deposited on the pad area. (b) Time profile of pulse voltages of various widths sent from a pulse generator with a 1 V output voltage and delivered to the device circuit as measured by an oscilloscope. (c) Angular-dependent Hall resistance measured for a switching device at various in-plane magnetic fields.

**Figure 2.** (a) Schematics of (left) field alignment ( $\mu_0 H = 0.5 \text{ T}$ ,  $\alpha = 30^\circ$ ) of AFM sublattice moments via spin-flop transition, and (right) electrical pulse switching of AFM moments to align along  $x$ -axis. (b)-(e) Electrical switching of Fe<sub>2</sub>O<sub>3</sub> spins for various pulse widths at a pulse current density ( $J_p$ ) above the threshold. The measurement series is as follows: First, an in-plane magnetic field is ramped up to 0.5 T and back to zero. Then, the Hall resistance is measured repeatedly for five times (blue points). Next, before each of the five red points, a current pulse is sent through the sample, followed by a Hall resistance measurement. Subsequently, the magnetic field is again applied before the next set of blue points to realign the Néel vector. Any linear resistance drift is subtracted. (f) Electrical switching with the same pulse parameters as in (b) for  $\Delta t = 0.3 \text{ ns}$  but with a lower alignment field of 0.1 T, which shows no detectable Hall resistance change.

**Figure 3.** (a) Dependence of Hall resistance on pulse current density for various pulse widths. Before each trace the moments are aligned with a 0.5 T magnetic field, after which pulses of increasing current density are sent through the sample. Data shown are the Hall resistances measured after each pulse. (b) Dependence of threshold switching current density on pulse width, where the threshold switching current density is defined as the pulse current density after which the change of  $|R_{xy}|$  is  $>3 \text{ m}\Omega$  in (a). Error bars are calculated from the standard deviation of 5

measurements per point. (c) Switching rate ( $1/\Delta t$ ) versus threshold switching current density. The higher frequency region at 1 GHz and above is fitted with  $J_{th} = J_{th0} + Q/\Delta t$  to show the  $1/\Delta t$  dependence in this regime. (d) Maximum temperature rises simulated in COMSOL for threshold pulse current densities.

## References:

1. J. Železný, P. Wadley, K. Olejník, A. Hoffmann and H. Ohno, "Spin transport and spin torque in antiferromagnetic devices," *Nat. Phys.* **14**, 220-228 (2018).
2. V. Baltz, A. Manchon, M. Tsoi, T. Moriyama, T. Ono and Y. Tserkovnyak, "Antiferromagnetic spintronics," *Rev. Mod. Phys.* **90**, 015005 (2018).
3. T. Jungwirth, X. Marti, P. Wadley and J. Wunderlich, "Antiferromagnetic spintronics," *Nat. Nanotechnol.* **11**, 231 (2016).
4. R. Cheng, J. Xiao, Q. Niu and A. Brataas, "Spin Pumping and Spin-Transfer Torques in Antiferromagnets," *Phys. Rev. Lett.* **113**, 057601 (2014).
5. T. Satoh, R. Iida, T. Higuchi, M. Fiebig and T. Shimura, "Writing and reading of an arbitrary optical polarization state in an antiferromagnet," *Nat. Photonics* **9**, 25 (2015).
6. P. Wadley, B. Howells, J. Zelezny, C. Andrews, V. Hills, R. P. Campion, V. Novak, K. Olejnik, F. Maccherozzi, S. S. Dhesi, S. Y. Martin, T. Wagner, J. Wunderlich, F. Freimuth, Y. Mokrousov, J. Kunes, J. S. Chauhan, M. J. Grzybowski, A. W. Rushforth, K. W. Edmonds, B. L. Gallagher and T. Jungwirth, "Electrical switching of an antiferromagnet," *Science* **351**, 587 (2016).
7. M. Meinert, D. Graulich and T. Matalla-Wagner, "Electrical Switching of Antiferromagnetic Mn<sub>2</sub>Au and the Role of Thermal Activation," *Phys. Rev. Appl.* **9**, 064040 (2018).
8. X. F. Zhou, J. Zhang, F. Li, X. Z. Chen, G. Y. Shi, Y. Z. Tan, Y. D. Gu, M. S. Saleem, H. Q. Wu, F. Pan and C. Song, "Strong Orientation-Dependent Spin-Orbit Torque in Thin Films of the Antiferromagnet Mn<sub>2</sub>Au," *Phys. Rev. Appl.* **9**, 054028 (2018).
9. S. Y. Bodnar, L. Šmejkal, I. Turek, T. Jungwirth, O. Gomonay, J. Sinova, A. A. Sapozhnik, H. J. Elmers, M. Kläui and M. Jourdan, "Writing and reading antiferromagnetic Mn<sub>2</sub>Au by Néel spin-orbit torques and large anisotropic magnetoresistance," *Nat. Commun.* **9**, 348 (2018).
10. M. J. Grzybowski, P. Wadley, K. W. Edmonds, R. Beardsley, V. Hills, R. P. Campion, B. L. Gallagher, J. S. Chauhan, V. Novak, T. Jungwirth, F. Maccherozzi and S. S. Dhesi, "Imaging Current-Induced Switching of Antiferromagnetic Domains in CuMnAs," *Phys. Rev. Lett.* **118**, 057701 (2017).
11. X. Z. Chen, R. Zarzuela, J. Zhang, C. Song, X. F. Zhou, G. Y. Shi, F. Li, H. A. Zhou, W. J. Jiang, F. Pan and Y. Tserkovnyak, "Antidamping-Torque-Induced Switching in Biaxial Antiferromagnetic Insulators," *Phys. Rev. Lett.* **120**, 207204 (2018).
12. T. Moriyama, K. Oda, T. Ohkochi, M. Kimata and T. Ono, "Spin torque control of antiferromagnetic moments in NiO," *Sci Rep* **8**, 14167 (2018).
13. L. Baldrati, O. Gomonay, A. Ross, M. Filianina, R. Lebrun, R. Ramos, C. Leveille, F. Fuhrmann, T. R. Forrest, F. Maccherozzi, S. Valencia, F. Kronast, E. Saitoh, J. Sinova and M. Kläui, "Mechanism of Neel Order Switching in Antiferromagnetic Thin Films Revealed by Magnetotransport and Direct Imaging," *Phys. Rev. Lett.* **123**, 177201 (2019).
14. H. Meer, F. Schreiber, C. Schmitt, R. Ramos, E. Saitoh, O. Gomonay, J. Sinova, L. Baldrati and M. Kläui, "Direct Imaging of Current-Induced Antiferromagnetic Switching Revealing a Pure Thermomagnetoelastic Switching Mechanism in NiO," *Nano Letters* **21**, 114-119 (2021).
15. Y. Cheng, S. S. Yu, M. L. Zhu, J. Hwang and F. Y. Yang, "Electrical Switching of Tristate Antiferromagnetic Néel Order in *a*-Fe<sub>2</sub>O<sub>3</sub> Epitaxial Films," *Phys. Rev. Lett.* **124**, 027202 (2020).

16. P. X. Zhang, J. Finley, T. Safi and L. Q. Liu, "Quantitative Study on Current-Induced Effect in an Antiferromagnet Insulator/Pt Bilayer Film," *Phys. Rev. Lett.* **123**, 247206 (2019).
17. I. Gray, T. Moriyama, N. Sivadas, G. M. Stiehl, J. T. Heron, R. Need, B. J. Kirby, D. H. Low, K. C. Nowack, D. G. Schlom, D. C. Ralph, T. Ono and G. D. Fuchs, "Spin Seebeck Imaging of Spin-Torque Switching in Antiferromagnetic Pt/NiO Heterostructures," *Phys. Rev. X* **9**, 041016 (2019).
18. E. Cogulu, H. T. Zhang, N. N. Statuto, Y. Cheng, F. Y. Yang, R. Cheng and A. D. Kent, "Quantifying Spin-Orbit Torques in Antiferromagnet--Heavy-Metal Heterostructures," *Phys. Rev. Lett.* **128**, 247204 (2022).
19. Y. Cheng, E. Cogulu, R. D. Resnick, J. J. Michel, N. N. Statuto, A. D. Kent and F. Y. Yang, "Third harmonic characterization of antiferromagnetic heterostructures," *Nat. Commun.* **13**, 3659 (2022).
20. B. J. Jacot, G. Krishnaswamy, G. Sala, C. O. Avci, S. Vélez, P. Gambardella and C. H. Lambert, "Systematic study of nonmagnetic resistance changes due to electrical pulsing in single metal layers and metal/antiferromagnet bilayers," *J. Appl. Phys.* **128**, 173902 (2020).
21. C. C. Chiang, S. Y. Huang, D. Qu, P. H. Wu and C. L. Chien, "Absence of Evidence of Electrical Switching of the Antiferromagnetic Neel Vector," *Phys. Rev. Lett.* **123**, 227203 (2019).
22. A. Churikova, D. Bono, B. Neltner, A. Wittmann, L. Scipioni, A. Shepard, T. Newhouse-Illige, J. Greer and G. S. D. Beach, "Non-magnetic origin of spin Hall magnetoresistance-like signals in Pt films and epitaxial NiO/Pt bilayers," *Appl. Phys. Lett.* **116**, 022410 (2020).
23. Y. Cheng, S. S. Yu, A. S. Ahmed, M. L. Zhu, Y. Rao, M. Ghazisaeidi, J. Hwang and F. Y. Yang, "Anisotropic magnetoresistance and nontrivial spin Hall magnetoresistance in Pt/*a*-Fe<sub>2</sub>O<sub>3</sub> bilayers," *Phys. Rev. B* **100**, 220408 (2019).
24. E. Cogulu, N. N. Statuto, Y. Cheng, F. Y. Yang, R. V. Chopdekar, H. Ohldag and A. D. Kent, "Direct imaging of electrical switching of antiferromagnetic Neel order in *a*-Fe<sub>2</sub>O<sub>3</sub> epitaxial films," *Phys. Rev. B* **103**, L100405 (2021).
25. K. Garello, C. O. Avci, I. M. Miron, M. Baumgartner, A. Ghosh, S. Auffret, O. Boulle, G. Gaudin and P. Gambardella, "Ultrafast magnetization switching by spin-orbit torques," *Appl. Phys. Lett.* **105**, 212402 (2014).
26. H. Liu, D. Bedau, D. Backes, J. A. Katine, J. Langer and A. D. Kent, "Ultrafast switching in magnetic tunnel junction based orthogonal spin transfer devices," *Appl. Phys. Lett.* **97**, 242510 (2010).
27. N. H. D. Khang, T. Shirokura, T. Fan, M. Takahashi, N. Nakatani, D. Kato, Y. Miyamoto and P. N. Hai, "Nanosecond ultralow power spin orbit torque magnetization switching driven by BiSb topological insulator," *Appl. Phys. Lett.* **120**, 152401 (2022).
28. D. Bedau, H. Liu, J. Z. Sun, J. A. Katine, E. E. Fullerton, S. Mangin and A. D. Kent, "Spin-transfer pulse switching: From the dynamic to the thermally activated regime," *Appl. Phys. Lett.* **97**, 262502 (2010).

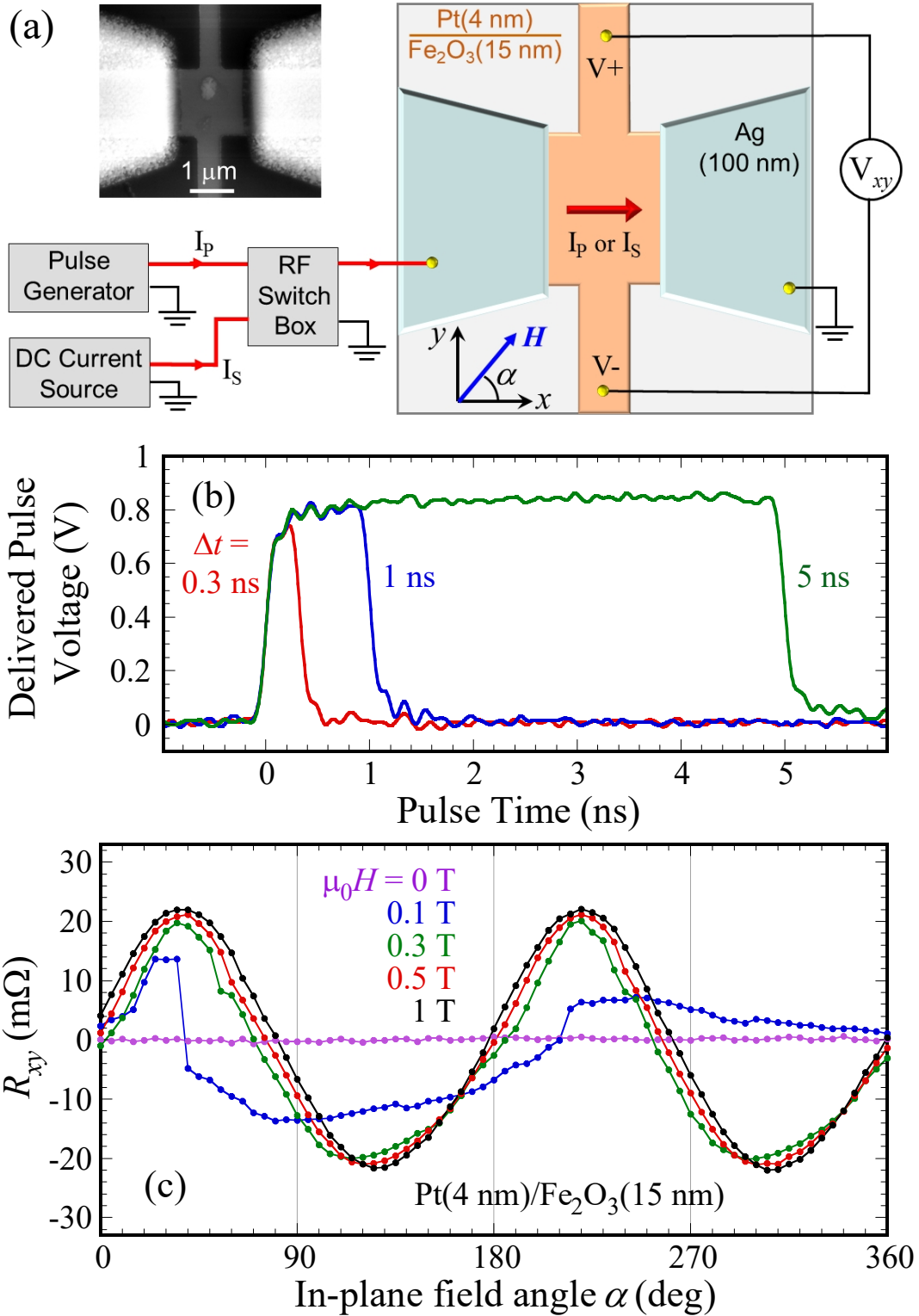


Figure 1.

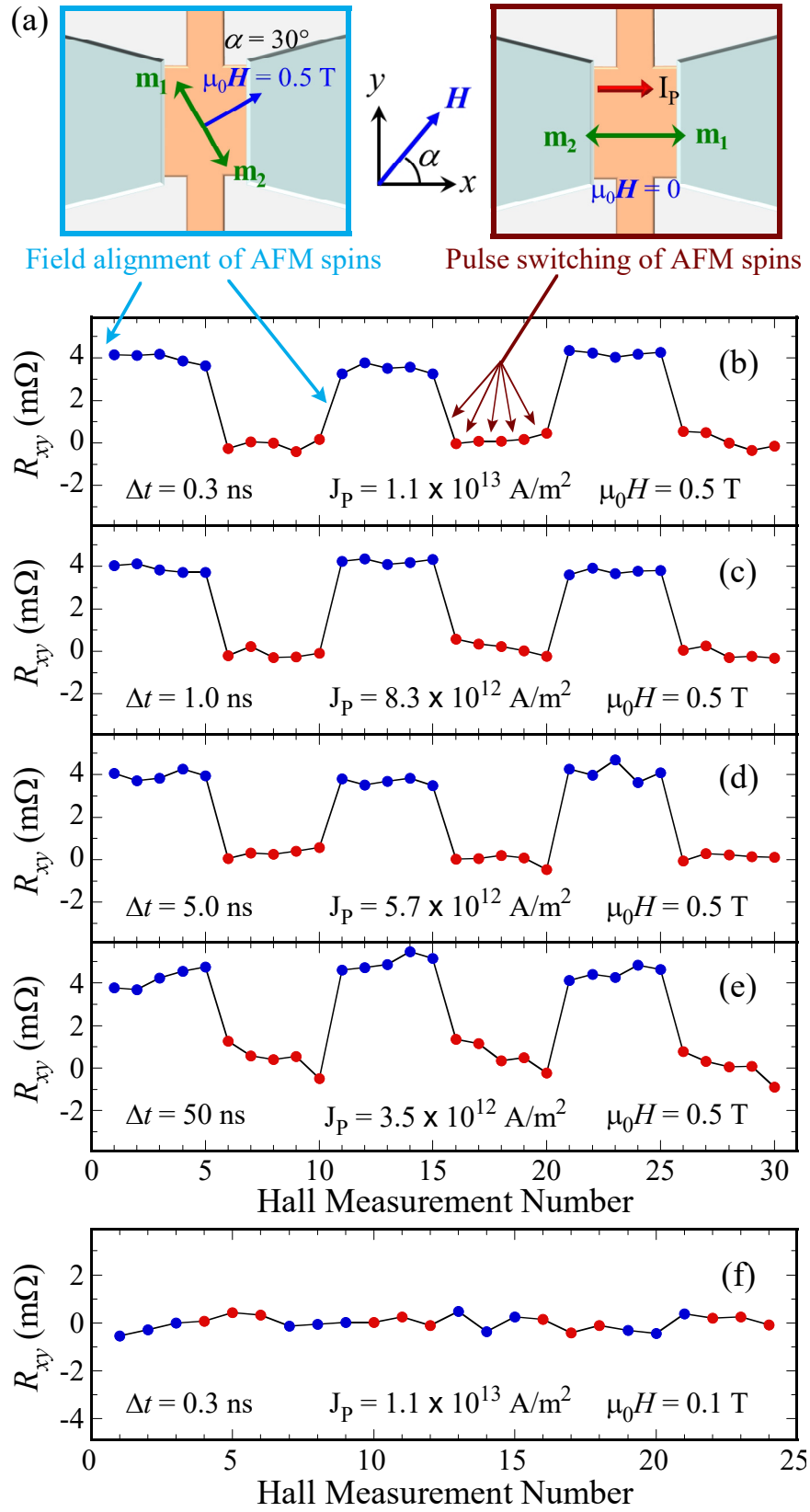


Figure 2.

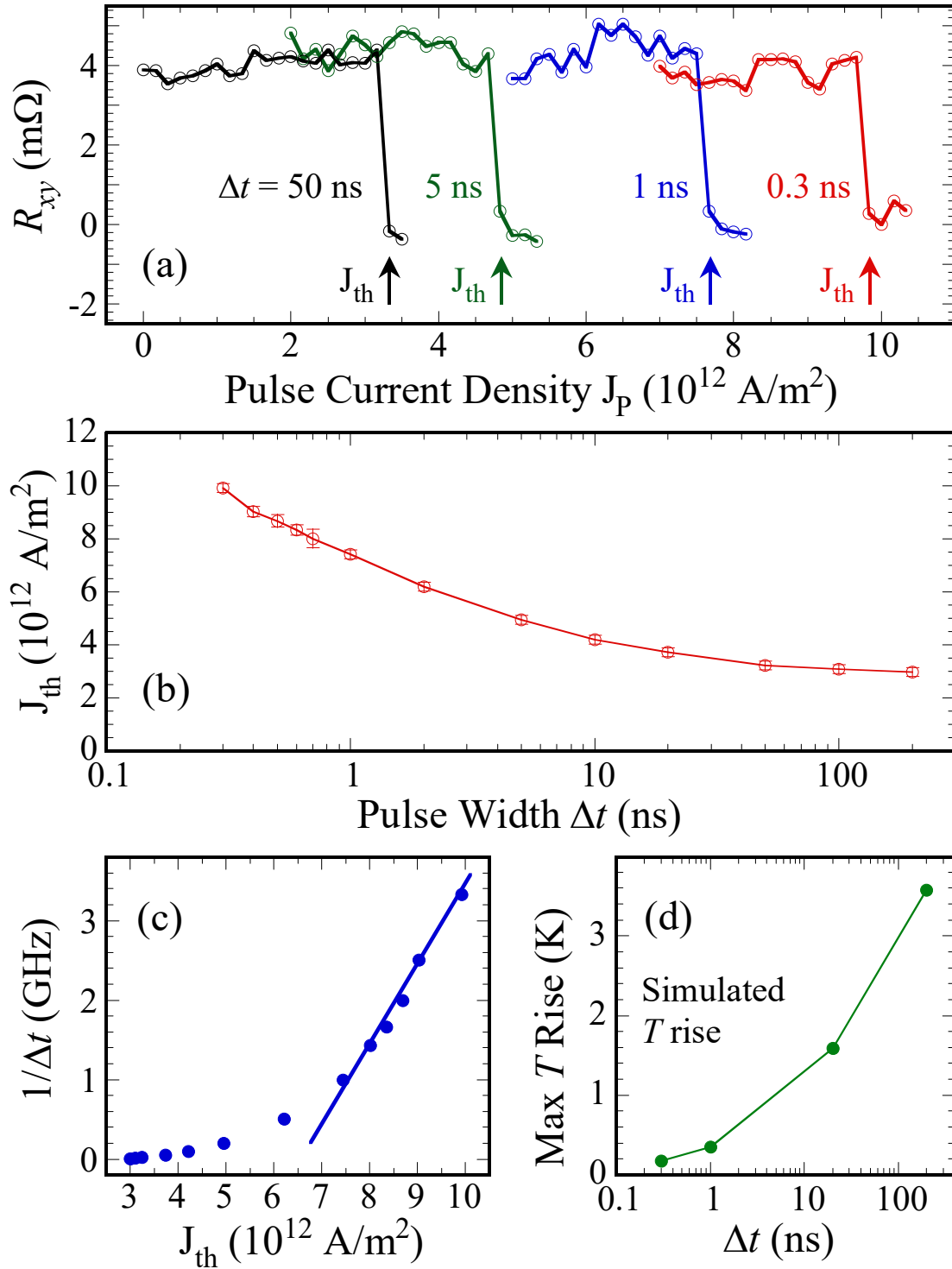


Figure 3.